ADVANCES IN APPLIED CERAMICS
2023, VOL. 122, NOS. 3–4, 181–196
https://doi.org/10.1080/17436753.2023.2227446

I·M3 Institute of Materials, Minerals & Mining
Taylor & Francis
Taylor & Francis Group

Localised surface modification of high-strength aluminium–alumina metal matrix composite coatings using cold spraying and friction stir processing

Wania Jibran[a], Priti Wanjara[b], Javad Gholipour Baradari[b], Maria Ophelia Jarligo[a] and André McDonald[a]

[a]Department of Mechanical Engineering, 10-230 Donadeo Innovation Center for Engineering, University of Alberta, Edmonton, Canada; [b]National Research Council Canada, Aerospace Research Center, Montréal, Canada

ABSTRACT

This study presents a novel approach for surface repairs of high-strength, cold-worked aluminium (Al) alloys, without negatively affecting the base material strength. Low-pressure cold spraying was used to fabricate Al–Al_2O_3 metal matrix composite overlays, with varying concentrations of Al_2O_3 deposited on an Al alloy. Friction stir processing (FSP) was employed to disperse and consolidate the overlay coating on the base material. The FSP was found to improve the Al_2O_3 particle distribution in the coating and reduce the mean free path between Al_2O_3 particles. The coating hardness increased after FSP. The post-FSPed overlays also exhibited lower wear rates compared to the as-sprayed condition. Remarkable improvement was observed in the tensile properties of the coatings, which were attributed to the improved dispersion of Al_2O_3 particles in the matrix, while the enhanced ductility was attributed to the possible grain refinement that occurred due to the recrystallisation of Al during FSP.

ARTICLE HISTORY
Received 17 November 2022
Revised 8 May 2023
Accepted 15 June 2023

KEYWORDS
Alumina; aluminium alloy; cold spray; friction stir processing; mechanical properties; metal matrix composite; repair overlays; coatings

Introduction

Aluminium (Al) alloys can be classified into two categories: heat treatable and non-heat treatable. The repair methodologies that exist for these alloys are limited or non-existent currently as they often introduce strength losses in the material, which prevent return of the part to service. For instance, non-heat treatable Al alloys, such as the 5xxx series, are strengthened by work-hardening to enhance their mechanical properties. Heat application to a work-hardened Al alloy causes the material to return to its annealed condition, reducing the strength significantly [1–4]. It is for these reasons that repairs of high-strength, cold-worked Al alloys remain a longstanding challenge, and presently these alloys are considered unrepairable. However, developing repair methodologies for cold-worked Al alloys is essential, as these alloys are frequently used as components in shipbuilding and off-shore platforms in marine industry, window frames and staircases in building and construction, and to make pressure vessels among others due to their excellent corrosion properties. They are also frequently used as airframes of modern aircrafts in the aerospace industry and engine radiators and wheels, etc. in the automotive industry, as well as in the defence sector for military vehicles, due to their high static tensile strength, moderate-to-high fatigue strength and low weight. Considering the diverse and broad application of cold-worked Al grades, an effective repair methodology would provide game changing advantages and agility to industry. Traditional repair techniques such as arc welding, thermal spray and laser deposition are still the most used in industries. The high heat input and temperature involved in such processes limit their repair capabilities, as they most likely create defects such as thermal deformation, oxidation inclusions and porosity. These traditional techniques could not be practically used to repair thin-walled components and complex shapes.

In the past few years, the cold spray technology, a metal additive process, has gained widespread attention in the repairs department of metal industries [5,6]. Cold spraying is a solid-state coating fabrication technology used to produce dense metal or metal matrix composite (MMC) coatings and overlays. During cold spraying, powder particles are accelerated to supersonic velocities using a carrier gas through a de Laval nozzle. The powder particles attain high kinetic energy as they exit the nozzle, which causes them to undergo severe plastic deformation upon impact and adhesion to the substrate to form the coating layers [7,8]. As implied by the name, cold spraying is a cold deposition process (0–700°C) that operates at temperatures that are lower than the melting point of the feedstock powder. Therefore, the deposited coatings are nearly devoid of oxidation, decarburization, metallurgical changes and residual thermal stresses [9,10]. Since cold spray is a solid-state deposition

CONTACT André McDonald andre.mcdonald@ualberta.ca Department of Mechanical Engineering, 10-230 Donadeo Innovation Center for Engineering, University of Alberta, 9211-116 Street NW, Edmonton, AB, Canada, T6G 1H9

process, interparticle bonding is most likely due to the mechanical interlocking of particles; hence the deposited coatings exhibit brittle behaviour under tensile loading [2].

Another low-heat input repair technique that has gained industrial attention is the friction stir processing (FSP), a derivative of the friction stir welding (FSW) process. The FSP is a solid-state surface modification process used to modify microstructures and improve the mechanical properties of metals and alloys. It has been reported that FSP causes grain refinement and creates high-angle grain boundaries in addition to breaking up of dendritic microstructures and creating refined uniaxial grains, which result in improvement of strength, ductility and fatigue properties of materials [3]. During FSP, a rotating cylindrical tool, with a larger diameter shoulder and smaller diameter pin (relative to FSW) is plunged into the material and then traversed along the workpiece surface. The tool exerts a downward force onto the material, which generates frictional heat and softens the material under the shoulder, while the rotation of the tool shoulder inside the material subjects the material to severe plastic deformation at high strain rates [11,12]. Since FSP is a solid-state process, it has the added benefit of not introducing as many metallurgical changes to the material as would be expected in traditional fusion-based welding processes, making it an attractive technology for improving and repairing metals and alloys.

Despite the lower heat input conditions, FSP still causes strength degradation in high-strength Al alloys due to precipitate dissolution for heat treatable grades (2xxx, 6xxx and 7xxx series), as well as dynamic recovery and recrystallisation in cold-worked (5xxx series) materials [12]. In an effort to remedy the reduction in strength, inclusion of ceramic particles into the material was previously explored in [3]. It was found that by introducing alumina (Al_2O_3) particles into cold-worked Al alloy (AA) 5083 and then dispersing the ceramic particles into the alloy through FSP, the strength losses that occurred during conventional FSP (i.e. without particle reinforcement) were recovered. This was accomplished by introducing several grooves into the base plate, inserting the ceramic particles and then traversing the FSP tool over the surface to disperse the ceramic particles into the base material. Though this approach improved the hardness and yield strength of the repaired section compared to the base material, it came with a penalty of a 50% decrease in the ductility. Another limitation of the method was in the mode of introducing ceramic particles into the material during FSP. This was a difficult process requiring several steps to ensure good compaction of the ceramic particles within the grooves and good dispersion of the ceramic particles in the base plate. Therefore, addressing these limitations represented key objectives to further developing an efficient and effective repair methodology that would also not compromise the mechanical performance of high strength, cold-worked Al alloys. Some researchers have explored the effects of FSP on cold-sprayed coatings and concluded that FSP enhanced the hardness, wear resistance, ultimate tensile strength (UTS) and elongation of the MMC coating significantly [9,12–15]. These enhancements were attributed to the improved distribution of ceramic material in the MMC coating following FSP.

Realising the distinct advantages of both solid-state processes, namely cold spraying and FSP, the inherently 'cold' operational conditions of the former would minimise heat input and microstructural changes to the base material during deposition of the coating overlay; then FSP would provide the advantage of enhancing consolidation, bonding and reinforcement homogeneity of the cold-sprayed coating overlay to maximise its performance and functionality. This combination of processing techniques has been found to be an effective method in fabricating ceramic-metal composites [16]. Therefore, this research study explored coupling cold-sprayed Al–Al_2O_3 MMC coatings with FSP as a hybrid repair methodology to develop material overlays with improved mechanical properties to restore geometric and functional properties of unrepairable, cold-worked AA5052-H32.

Experimental methods

Coating deposition

The substrate material used in this study was 3.2 mm-thick AA5052 plate (Metal Supermarket, Edmonton) with a H32 temper – work hardened by cold rolling and then stabilised by partial annealing to a quarter hard condition. The substrate alloy with chemical composition listed in Table 1, complies with ASTM product specifications.

Since the roughness of the substrate is an important factor for good adhesion between the coating and the substrate [15,17], the substrates were grit-blasted using an alumina-based abrasive (#24 alumina grit, Manus Abrasive Systems Inc., Edmonton, AB, Canada). The powders used to prepare the feedstock

Table 1. Composition of the substrate alloy AA5052–H32.

Element	Amount, %
Aluminium, Al	95.7–97.7
Chromium, Cr	0.15–0.35
Copper, Cu	<= 0.10%
Iron, Fe	<= 0.40
Magnesium, Mg	2.2–2.8
Manganese, Mn	<= 0.10
Silicon, Si	<= 0.25
Zinc, Zn	<= 0.10
Other, each	<= 0.05
Other, total	< = 0.15

materials for the coatings included commercially available pure Al powder (SST-A5001, CenterLine, Ltd., Windsor, ON, Canada) and commercially available Al_2O_3 powder (AMDRY 6060, Oerlikon Metco Inc., Westbury, NY, USA). The starting powders were mechanically blended by manual tumble mixing for 5 min. Figure 1 shows the scanning electron microscope (SEM) images of the Al (Figure 1(a)) and Al_2O_3 (Figure 1(b)) particles which exhibit irregular morphology. While the Al particles have smooth edges, the Al_2O_3 particles appear to be angular. Both powders had a diameter distribution between 15 and 45 micron, as provided by the supplier. Four different Al-based mechanical blends with Al_2O_3 content of 0 wt-%, 10 wt-%, 50 wt-% and 75 wt-% were investigated in this study.

The coating depositions were carried out using a low-pressure cold spray system (SST series P, CenterLine, Ltd., Windsor, ON, Canada) mounted on a robot (HP-20, Motoman, Yaskawa Electric Corp., Waukegan, IL, USA). Compressed air at 689 kPa (100 psi) was used as the carrier gas for the coating deposition at 300°C. The powder hopper of the cold spray control unit had an integrated vibrator system that kept the feedstock powders homogeneously blended as they enter the gas stream for ejection. A stand-off distance of 5 mm and nozzle traverse velocity of 4.5 mm s^{-1} was used. The applied nozzle (Ultilife™, Centerline Ltd., Windsor, ON, Canada) was a wear resistant stainless steel, and was recommended by the manufacturer as ideal for spraying pure and hard/abrasive materials, such as Al and Al_2O_3. It had a length of 120 mm, an entrance diameter of 4.46 mm and an exit diameter of 6.40 mm. Coatings with a thickness of approximately 2.5 mm were deposited.

Friction stir processing

The coated AA5052-H32 plates were secured to a FSP table (ISTIR PDS, MTS Systems Corporation, MN, USA) and a H13 tool steel, flat face cylindrical FSP tool of 13 mm diameter was traversed over the coating deposit at a constant speed of 9 mm s^{-1}, as illustrated in Figure 2. The rotational speed for the cylindrical tool was set to 1200 rotations per minute (RPM). The tool was operated with an axial force in a range between 6 and 10 kN, depending on the required depth of penetration. The FSP was conducted at ambient temperature.

Materials characterisation and testing

A SEM (Sigma, Zeiss, Cambridge, UK) was used to characterise the microstructure of the coated samples. The SEM was operated with an acceleration voltage of 15 kV and a working distance of around 6 mm. From the SEM images of the coating cross-section, the Al_2O_3 particle content, porosity, average particle size and mean free path between the reinforcing Al_2O_3 particles were characterised using an image processing

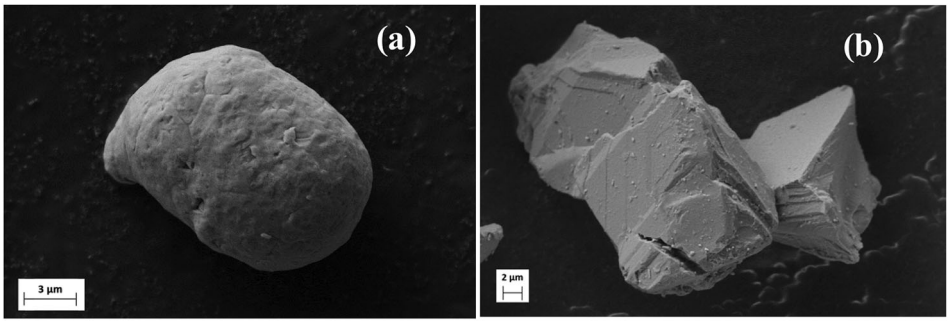

Figure 1. SEM images of the starting (a) Al and (b) Al_2O_3 powders.

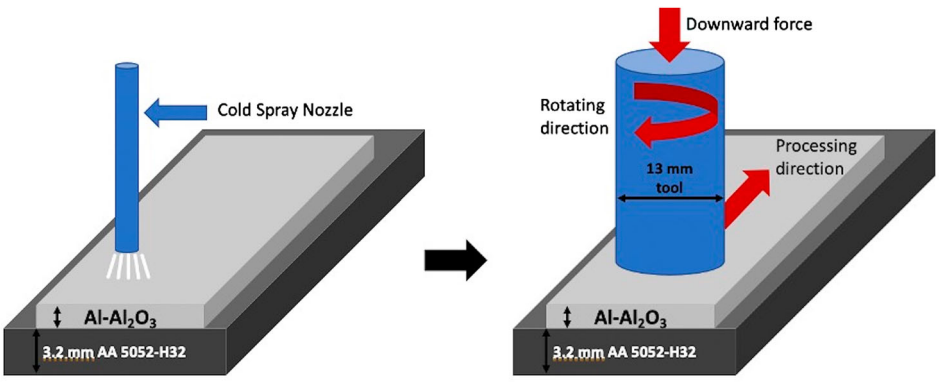

Figure 2. Schematic of FSP performed for Al–Al_2O_3 MMC coatings.

software, ImageJ (National Institute of Health and the Laboratory for Optical and Computational Instrumentation, Maryland, USA). The volume fraction of Al_2O_3 in the coating was then converted to weight fraction using the densities of the powders. The mean free path is a measurement of the distance between the nearest Al_2O_3 particles in the coating. The mean free path was evaluated using Equation (1) as follows [8]:

$$\lambda = \frac{1 - v_r}{N_L}, \tag{1}$$

where v_r is the volume fraction of the reinforcing Al_2O_3 particles and N_L is the number of particle intercepts per unit length. For all microstructural calculations, a minimum of four SEM images were used with at least five areas of interest ($n = 20$).

Coating hardness was measured using a microhardness testing machine (Buehler VH1202, Lake Bluff, IL, USA) with a Vickers indenter, in accordance with the ASTM E384-17 standard [18]. A minimum of 15 ($n = 15$) measurements were taken on the polished cross-sections of each coating sample at different locations on the substrate close to the interface, on the substrate-coating interface and on the coating with a load of 1 kgf and dwell time of 10 s.

Dry abrasion and high-stress abrasion testing were performed for all coating samples as per ASTM G65-16e1 [19] and ASTM standard B611-13 [20], respectively. For dry abrasion testing (ASTM G65-16e1) using silica sand, procedure E (1000 revolutions) was selected with the wheel rotational speed of 200 RPM, a force of 130 N and sliding distance of 718 m. A modified procedure (25 revolutions) was selected for the high stress or wet abrasion testing (ASTM standard B611-13) using alumina grits, with a wheel rotational speed of 100 RPM and sliding distance of 13.3 m. Three samples ($n = 3$) were tested for each coating composition. The wear rate (W) in mm^3/N-m was calculated by dividing the volume loss (Δv), in mm^3, by the applied load (P), in Newton, and the sliding distance (s), in m, as shown in Equation (2):

$$W = \frac{\Delta V}{P * s}. \tag{2}$$

Uniaxial tensile testing was conducted in a universal testing system (Instron 5966, Norwood, MA, USA). Tensile test specimens of the coating samples were prepared according to ASTM Standard E8/E8M-13a [21] using a wire-based electrical discharge machine (EDM) (Agie Progress V4, Agie, 1242 Satigny, Switzerland) to extract the coatings from the substrates. The samples were machined to a sub-sized standard geometry with gauge dimensions of 25 mm in length × 6 mm in width and a thickness of 1.1 mm. The tensile specimens were loaded at a rate of 0.0003 mm s^{-1}, which placed the test condition in the quasi-static loading regime. Digital image correlation (DIC) was used to compute the strains in the coating samples during tensile testing [8]. The strains were measured by capturing the deformation of the specimens *in situ* using a Promon U750 High Speed Camera (AOS Technologies AG, Taefernstrasse 20 CH-5405 Baden-Daettwil, Switzerland) at 100 frames s^{-1}, which produced time-stamped images of the tested specimens. The images were loaded into a DIC software Vic 2D 6 (Correlation Solutions, Irmo, SC, USA), and a mesh was generated for the specimens. To achieve reliable data from DIC, a high-quality speckle pattern is required on the specimens. To generate the speckle pattern on the test specimens, an ultra-fine Harder and Steenbeck Infinity airbrush (Harder and Steenbeck Gmbh, Norderstedt, Germany) was used with a spray needle diameter of 0.15 mm. To achieve a high-contrast image, high-intensity LEDs were used. An area of interest was determined on the specimen surface where the strain fields were calculated. The mesh size suggested by the software was 25 by 25 pixels. The mesh subsets were digitally tracked by the software in the subsequent time-stamped images to determine the strain in the specimen. The failure strain found using DIC and the failure stress from the tensile testing machine were matched to reconcile all the corresponding stresses and strains to develop stress–strain curves. Toughness, which is the amount of energy per unit volume that is absorbed by the material prior to rupturing, was obtained by integrating the area under the stress–strain curves.

Results and discussion

Microstructural changes

MMC coatings were fabricated by depositing powder blends containing 10, 50 and 75 wt-% Al_2O_3. As shown in Figure 3, these produced coating overlays containing 4.6 ± 0.8 wt-% ($n = 3$), 22.9 ± 0.6 wt-% ($n = 3$) and 34.6 ± 2.9 wt-% ($n = 3$) Al_2O_3, respectively, which will be hereafter referred to as 5, 23 and 35 wt-% Al_2O_3, respectively. The fluid dynamics law, $V \propto 1/(d\rho)^{1/2}$, states that the mean velocity, V of a particle is inversely proportional to the square root of its diameter, d and density, ρ. While the particle size ratio of the starting Al_2O_3-to-Al powders is equal to 1, the material density ratio is equal to 1.5. This implies that the Al_2O_3 particles travel much slower than the Al particles resulting in lower amounts of Al_2O_3 compared to Al in the coating matrix. Similar results were found by Hodder et al. [9] and Irissou et al. [22]. Moreover, it is hypothesised that the rebounding of ceramic particles from the substrate decreased the deposition efficiency due to inability of the Al_2O_3 particles to deform plastically during impact

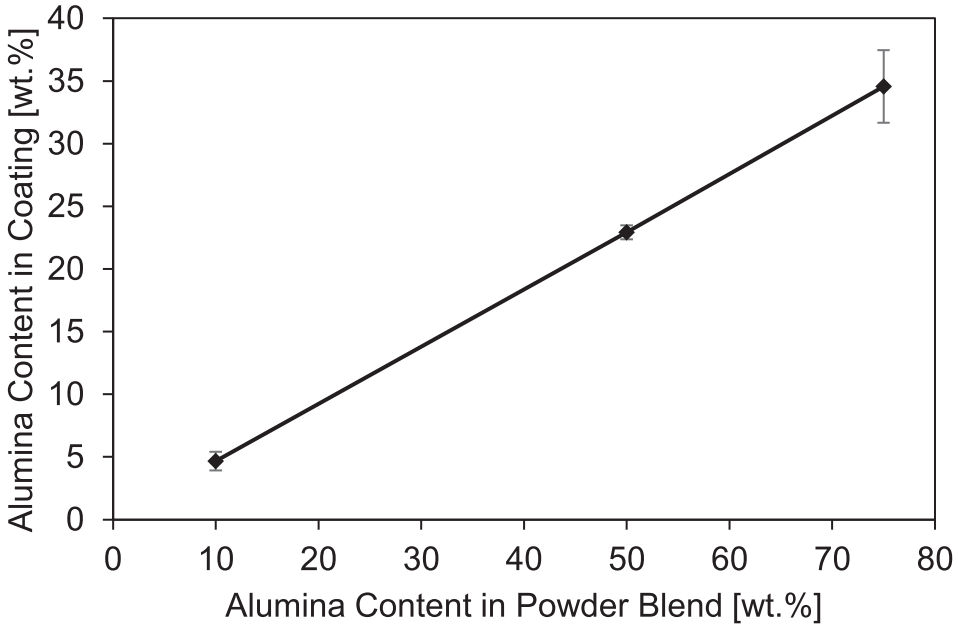

Figure 3. Plot of Al_2O_3 content in the powder blend versus that in the coating.

[23]. The obtained coating thicknesses were about 2 mm.

Figure 4 shows the optical microscope images of the as-sprayed (Figure 4(a and -b)) and post-FSPed coatings (Figure 4(c and d)). It was found that the Al_2O_3 particles fragmented to smaller sizes for the 23 wt-% and 35 wt-% coatings due to the impact forces during cold spray deposition (Table 2). Fracture of the Al_2O_3 particles during deposition improved the particle distribution in the Al matrix, which is reflected by the decreases in the Al_2O_3 particle size and mean free paths for the different coating samples, as illustrated in Figure 5. Following FSP, the Al_2O_3 particles appeared more refined and evenly distributed through the Al matrix. The level of dispersion of Al_2O_3 increased after FSP and the Al_2O_3 particles appeared smaller and with higher circularity post-FSPed compared to their initial shape, which contained more sharp edges. This refinement and redistribution following FSP are due to the shear forces exerted by

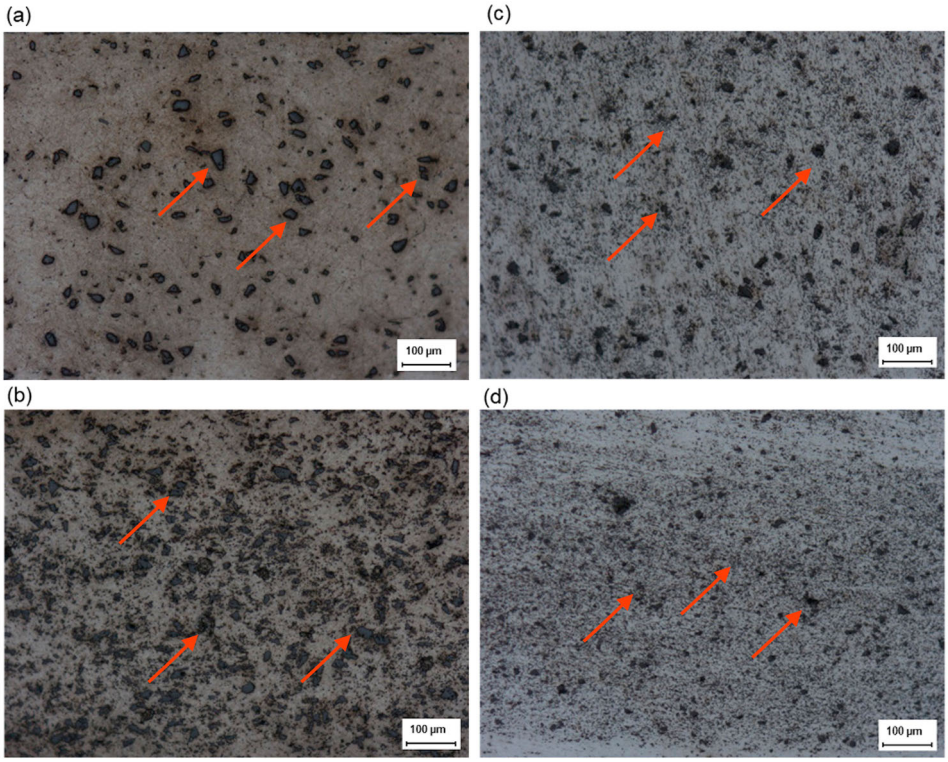

Figure 4. Images of the coating cross-sections for as-sprayed coatings (a) 5 wt-% Al_2O_3, (b) 23 wt-% Al_2O_3 and post-FSPed, (c) 5 wt-% Al_2O_3 and (d) 23 wt-% Al_2O_3. Alumina particles are indicated by the red arrows.

Table 2. Al_2O_3 particle size in the coating for both as-sprayed and post-FSPed coatings.

	Alumina particle size in coating	
Wt-% Al_2O_3	As-sprayed size [μm^2]	Post-FSPed size [μm^2]
5	144.2 ± 0.9	60.5 ± 0.1
23	97.2 ± 0.2	47.6 ± 0.1
35	34.7 ± 0.2	14.7 ± 0.0

the FSP tool on the material during the stirring [2]. The stirring action of the tool fractured the edges of the Al_2O_3 particles, leaving smaller and rounder particles. The improved distribution of Al_2O_3 particles is reflected in the mean free path measurements, with the lowest mean free path of 10 μm observed in the post-FSPed coating containing 35 wt-% Al_2O_3.

Figure 6 shows the coating porosity as a function of Al_2O_3 content for the as-sprayed and post-FSPed samples which reveals that the porosity decreased with increasing Al_2O_3 content in the coating. The highest porosity of 5.3 ± 0.3% ($n = 6$) corresponded to the as-sprayed pure Al coating and is attributed to the low density and irregular morphology of the Al powder particles, which can promote gas entrapment during the deposition process and, thereby, create pores [9]. The reduction in porosity with increasing Al_2O_3 content can be explained by the peening effect on the coating due to repeated impact of the hard Al_2O_3 particles on the previously deposited MMC layer, which collapses pores and produces a highly dense MMC coating with reduced porosity. The porosity in the coating is reduced further after FSP, as the shear force exerted during the stirring of the tool can cause the pores to collapse and promote metallurgical bonding between the particles [15]. The post-

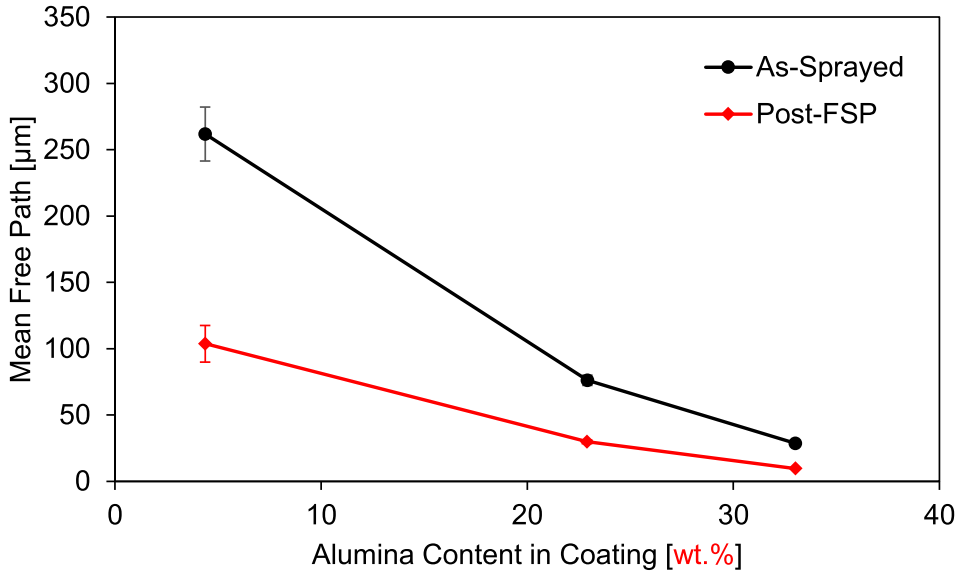

Figure 5. Mean free path between the Al_2O_3 particles versus the Al_2O_3 content in the coating.

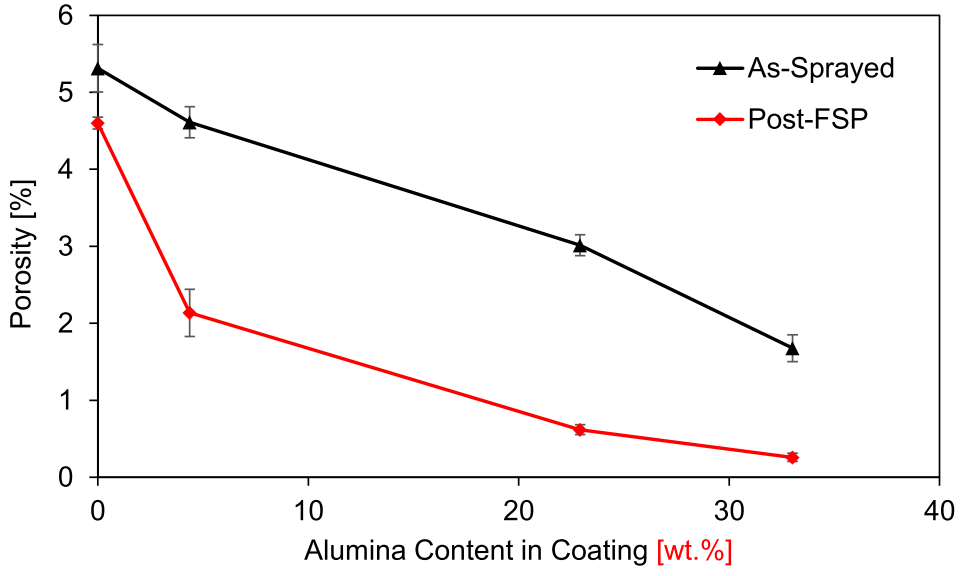

Figure 6. Approximate coating porosity versus the Al_2O_3 content in the coating.

FSPed coating containing 35 wt-% Al_2O_3 exhibits the lowest porosity of 0.3 ± 0.1% ($n = 6$).

Mechanical behaviour

Coating hardness

Figure 7 shows increasing coating hardness with increasing Al_2O_3 content in the coating. Significant increase in hardness was observed for coatings containing 23 wt-% and higher Al_2O_3. It was observed that FSP further increased the hardness of the cold-sprayed MMC coatings. The pure Al coating experienced an increase in hardness of 28% after FSP. The greatest improvement however was exhibited by the coating which contained 35 wt-% Al_2O_3 that yielded a hardness value that is 22% higher than the hardness for bulk AA5052-H32. The dramatic increase in hardness with FSP and increasing Al_2O_3 content can be explained by the uniform distribution and refinement of Al_2O_3 particles in the post-FSPed coatings. The FSP significantly increased MMC coating hardness by decreasing the mean free path of reinforcing particles. It is observed in Figure 8 that there is a near linear relationship between mean free path of Al_2O_3 particles and coating hardness when the mean free path is less than 100 µm. Therefore, it can be concluded that coating hardness, in this case, increases significantly when the mean free path falls below a certain threshold value, in this case 100 µm. In coating matrices reinforced with a higher fraction of the harder Al_2O_3

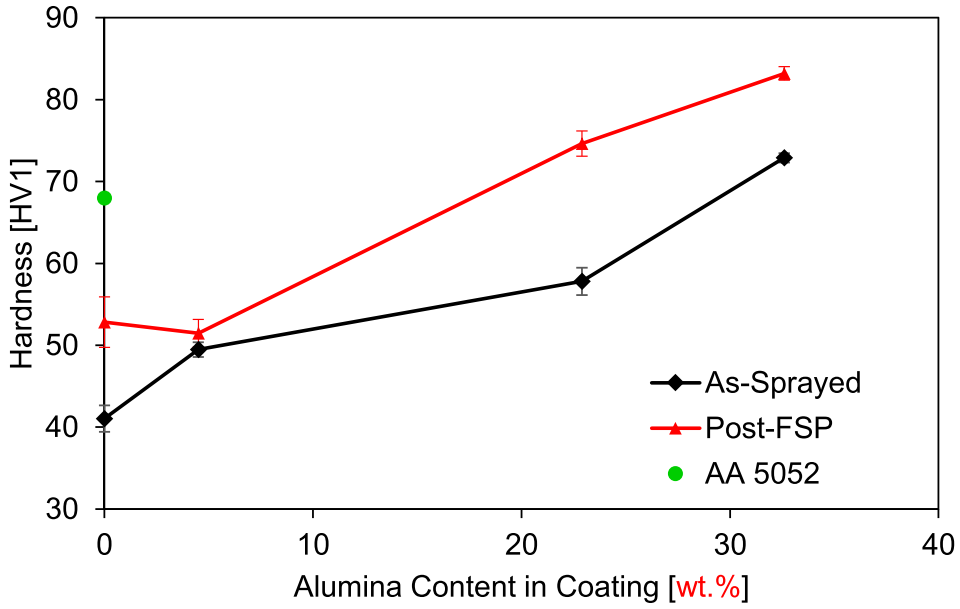

Figure 7. Relationship between coating hardness and Al_2O_3 content.

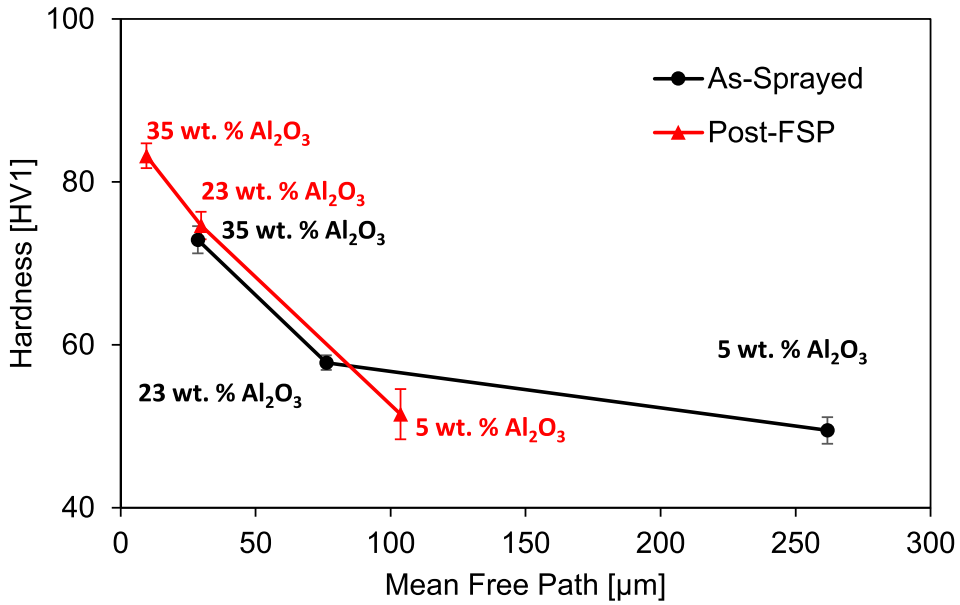

Figure 8. Relationship between the mean free path between Al_2O_3 particles and coating hardness.

particles, the Al_2O_3 particles share the axial load applied during hardness testing, thereby reducing the load transferred to the coating matrix and resulting in improved coating hardness.

During hardness measurements, the sharp indenter may be applied either onto the hard Al_2O_3 grains or onto the soft Al matrix, and the crack initiation and hardness values would vary significantly. However, after FSP, where the coating structure became highly homogenised and compacted compared to the as-cold-sprayed coatings, the hardness data should also be significantly more uniform and consistent.

Thermomechanical conditions such as temperature, strain and strain rate during FSP are sufficient to cause recrystallizstion in the AA5052-H32 base material. Thus, it is important to determine if the coating and base material interface are affected following FSP. As illustrated in Figure 9, for the as-sprayed coating samples, the substrate and interface hardness remained constant at around 74 HV1. The substrate hardness for the post-FSPed coating with 5 wt-% Al_2O_3 and 35 wt-% Al_2O_3 exhibited minor reduction in hardness which can be attributed to thermal softening that is introduced into the interface and substrate during FSP. Since the material was subjected to higher normal forces while processing the 35 wt-% Al_2O_3 coating relative to the 5 wt-% Al_2O_3 coating, due to the higher hardness of the 35 wt-% Al_2O_3 coating, the heat input into the processing region was increased which led to greater thermal softening at the interface and substrate of the former relative to the latter. As the FSP parameters for this study were tailored to ensure suitable mixing and consolidation of the coating, whilst managing overheating, another approach will need to be introduced to mitigate softening effects in the substrate that result from the higher heat input for harder deposits.

Tensile behaviour

Figure 10 shows the average stress–strain curves generated during tensile testing of the as-sprayed and post-FSPed coatings. As observed in Figure 10(a), the as-sprayed samples exhibited limited plastic deformation before experiencing failure. Following FSP as shown in Figure 10(b), it can be observed that the coatings undergo significant plastic deformation before experiencing failure, which is analogous to the behaviour of metals and metal alloys. Therefore, analysing the difference between the response of the as-sprayed and post-FSPed coatings, it can be concluded that FSP has a great improvement effect on the tensile response of as-sprayed Al–Al_2O_3 coatings.

Figure 11 shows an increase in the UTS of the as-sprayed and post-FSPed coatings with different Al_2O_3 fractions. Post-FSP, each coating exhibited higher UTS values compared to their as-sprayed state. The pure Al coatings exhibited the largest improvement (more than double) in UTS. This significant increase in the UTS can be attributed to the strain hardening and consolidation effects of FSP on the as-sprayed coating. Increasing the Al_2O_3 content in the coating improves the coating strength by reducing

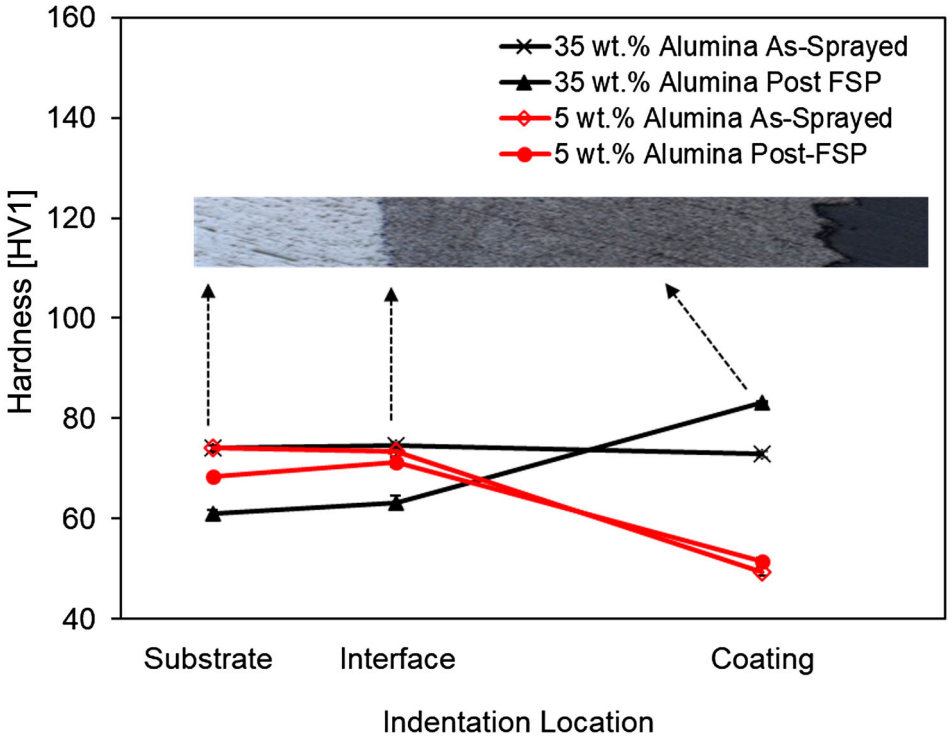

Figure 9. Hardness map tracking the hardness changes between the substrate, interface and coating for the post-FSPed samples with 5 wt-% Al_2O_3 and 35 wt-% Al_2O_3. The coating cross-section image is for the post-FSPed coating with 35 wt-% Al_2O_3 and is only displayed to indicate the indent location.

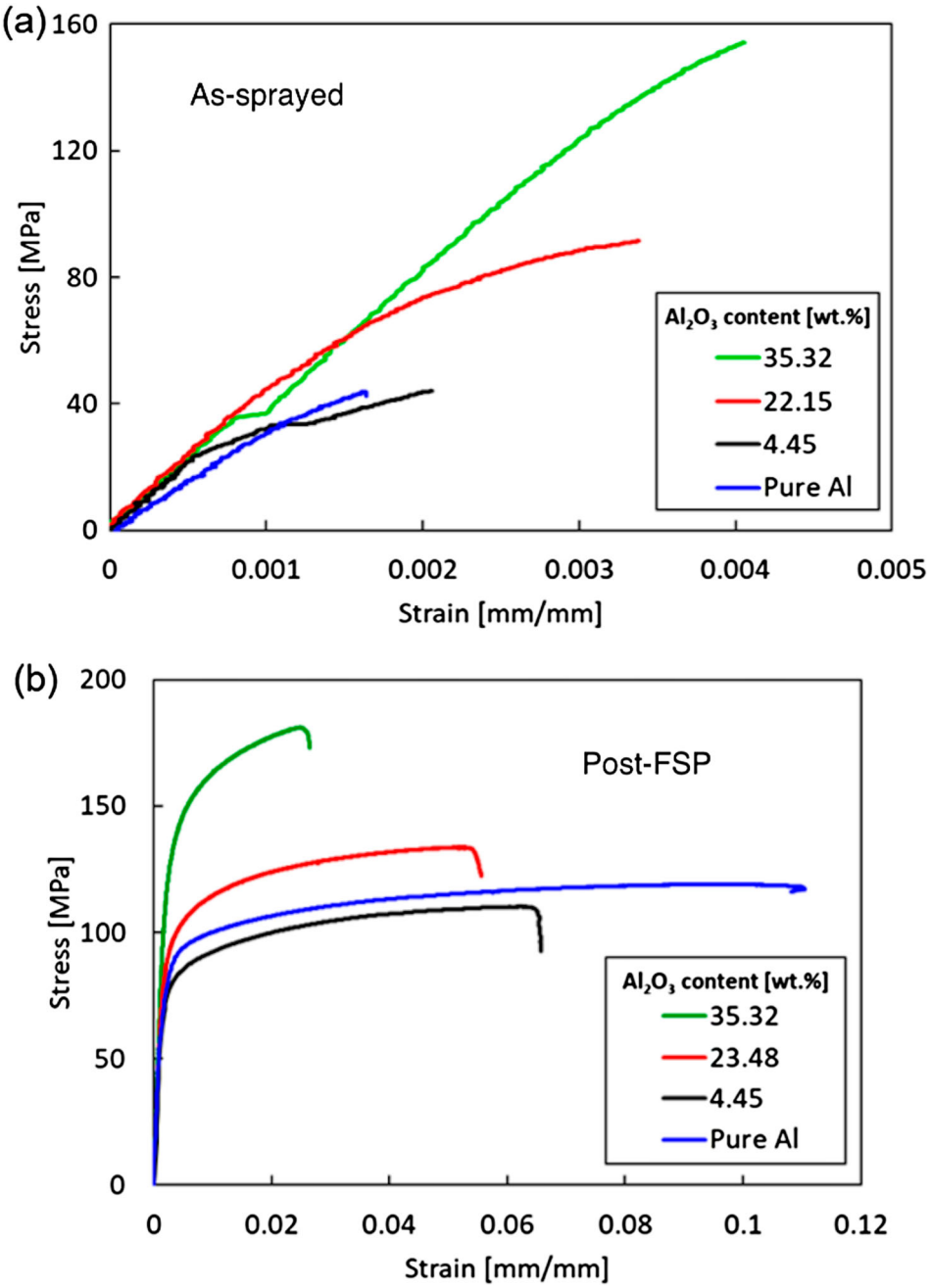

Figure 10. Average tensile stress versus tensile strain for (a) as-sprayed and (b) post-FSPed coatings. The legend indicates the wt-% Al_2O_3 for each sample.

physical defects such as pores in the coating and FSP further reduces coating porosity. The strength of the coatings improves with reduced porosity, as the likelihood of void nucleation and crack propagation is reduced. FSP also introduces microstructural refinement, which causes the mean free path between Al_2O_3 particles to decrease, improving the UTS of the coating, as it increases the dislocation density in the material. Physical defects in the material, such as pores often dominate the material's response to external loading. The UTS difference between the pure Al, 5 wt-% Al_2O_3 and 23 wt-% Al_2O_3 is not as dramatic as the difference between the 23 wt-% Al_2O_3 and 35 wt-% Al_2O_3 samples. This is because for all the coatings with less than 23 wt-% Al_2O_3, despite the microstructural refinement of the Al_2O_3 particles, the coating response to external loading is also affected by the porosity in the coatings, which for these samples, is greater than 1% (Figure 6). Therefore, despite the improvement in Al_2O_3 distribution in the coating material, the UTS does not increase as dramatically. As the coating porosity is reduced to values lower than 1%, which is the case for the 35 wt-% Al_2O_3 coatings, the UTS increases dramatically as it is no longer affected by physical defects.

In order to compare the elongation response of the coatings, both toughness, which is the energy absorbed to failure per unit volume of the material, and failure strain were analysed for the as-sprayed and post-FSPed coatings, as shown in Figures 12

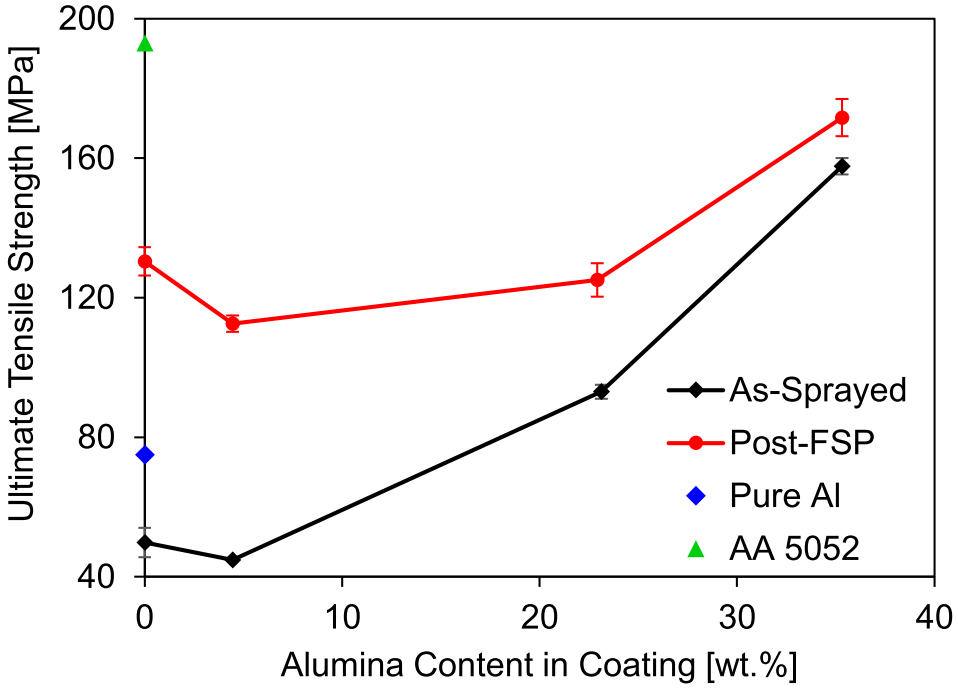

Figure 11. Relationship between ultimate tensile strength and Al_2O_3 content for as-sprayed and post-FSPed coatings.

and 13, respectively. For the as-sprayed condition, the energy absorbed to failure increased with increasing amounts of Al_2O_3 in the coating. The low elongation and toughness of as-sprayed coatings can be attributed to the nature of the cold spray deposition process. Since mechanical bonding is the predominant bonding mechanism, as opposed to metallurgical bonding, cold-sprayed coatings often face issues of embrittlement and exhibit poor elongation due to the weak interparticle bonding [8]. It was also observed that the failure strain increased with increasing Al_2O_3 content for the as-sprayed coatings. This can be attributed to the reduced porosity that coatings with Al_2O_3 exhibit. The failure strain for post-FSPed coatings increased by an order of magnitude compared to the as-sprayed coatings. The energy absorbed to failure also increased by an order of magnitude. These remarkable improvements in the coating elongation and toughness can be attributed to the consolidating and compacting effects of FSP, which lead to a denser, less porous coating, in addition to improved metallurgical bonding between the coating particles [24]. Another reason for this considerable improvement in the elongation following FSP can be attributed to the conditions of thermoplastic deformation at high strain rates that are well-known for recrystallising

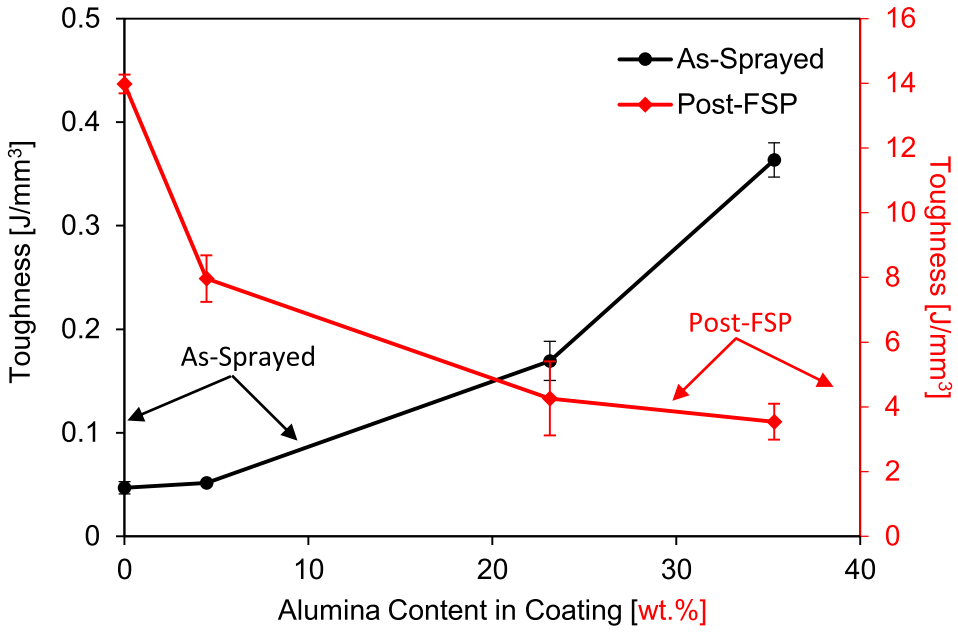

Figure 12. Relationship between coating toughness and Al_2O_3 content for as-sprayed and post-FSPed coatings.

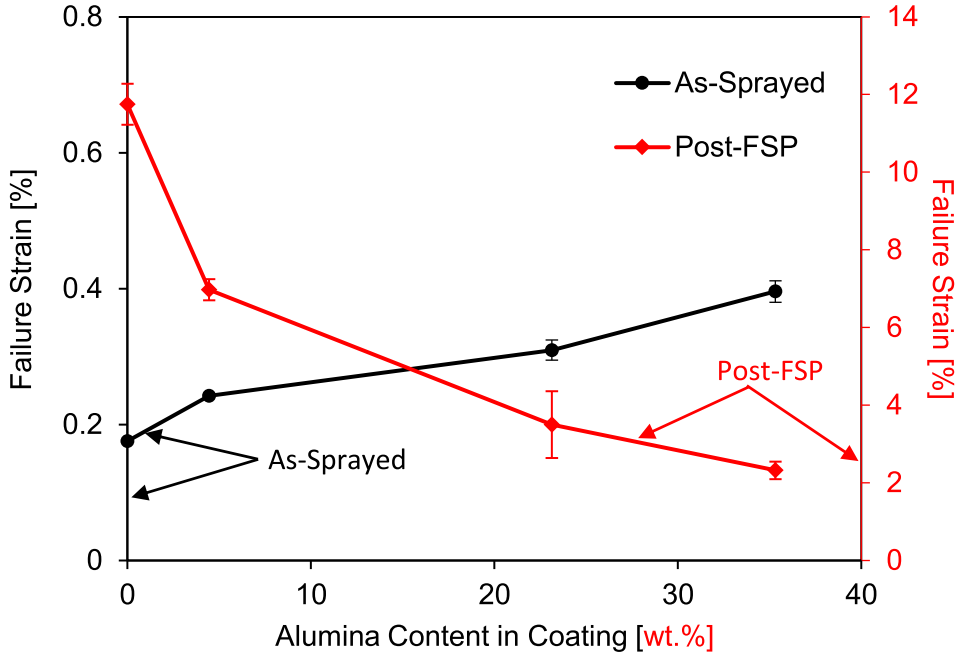

Figure 13. Relationship between failure strain and Al_2O_3 content for as-sprayed and post-FSPed coatings.

Al at the FSP nugget also known as stir zone, and grain refining the material. Specifically, recrystallisation of Al in the metallic matrix during FSP leads to the nucleation of strain-free grains with different orientations, and their refined nature increases the amount of grain boundaries (and the grain boundary area). As each grain boundary hinders dislocation motion by acting as a slip plane for dislocation movement, dislocation pile up occurs (at the grain boundaries) and, in turn, increases the stresses and energy needed for the fracture path to cross grain boundaries; thus, Al recrystallisation during FSP is known to improve both the strength and ductility (elongation and toughness) of the material [17]. It should be noted that the ceramic Al_2O_3 does not exhibit recrystallisation at cold spray and FSP temperature conditions. It is also observed that the failure strain decreases with increasing Al_2O_3 content for the post-FSPed coatings. This behaviour can be attributed to the effects of Al_2O_3 particles, which increase the dislocation density in the coating, hindering deformation in the material, which leads to reduced elongation and failure strain in post-FSPed coatings with high Al_2O_3 content. However, despite this reduction in elongation, the coating elongation of the post-FSPed coating containing 35 wt-% Al_2O_3 is still six times greater than that of the as-sprayed coating of the same composition.

Fracture surface analysis

The SEM images of the fracture surface of the as-sprayed and post-FSPed coatings are illustrated in Figure 14. For the as-sprayed coatings, the fracture surface exhibited a very porous microstructure and the presence of distinct particle boundaries. In Figure 14 (a–d), the individual Al and Al_2O_3 particle splats can be observed on the fracture surface, which proves the predominance of weak mechanical bonding between particles in the coating. This explains the inferior elongation behaviour for the as-sprayed coatings, as porosity can accelerate void nucleation and crack propagation. The weak interparticle bonding leads to accelerated and/or premature failure in the coating, as the brittle fracture occurs along particle interfaces rather than through them. The presence of Al_2O_3 particles on the fracture surface also gives evidence of weak bonding between Al–Al_2O_3 particles that causes the failure to occur around the Al_2O_3 particles. The absence of dimples, the evidence of matrix particle separation and the presence of porosity are all indicative of premature failure [24], which is reflected in the stress–strain curves for the as-sprayed coatings (see Figure 10). After FSP, the fracture surfaces of the coatings, as shown in Figure 14 (e–f), here exhibited a considerable amount of equiaxed and shear dimples on the surface. Unlike the as-sprayed coatings, the matrix particle separation and particle interfaces have disappeared in the post-FSPed MMC, and a dimpled rupture was observed with fracture occurring through the particles rather than between them. A dimple rupture is indicative of stronger interparticle bonding in the matrix and ductile fracture, which can be attributed to the occurrence of Al recrystallisation in the matrix, as discussed in the previous section. It was also observed that the dimples were larger for the post-FSPed coating with 5 wt-% Al_2O_3 and smaller for the post-FSPed coating with 35 wt-% Al_2O_3. This can be attributed particle-stimulated nucleation that increases the local lattice misorientations around the particle during thermoplastic deformation [24]; these

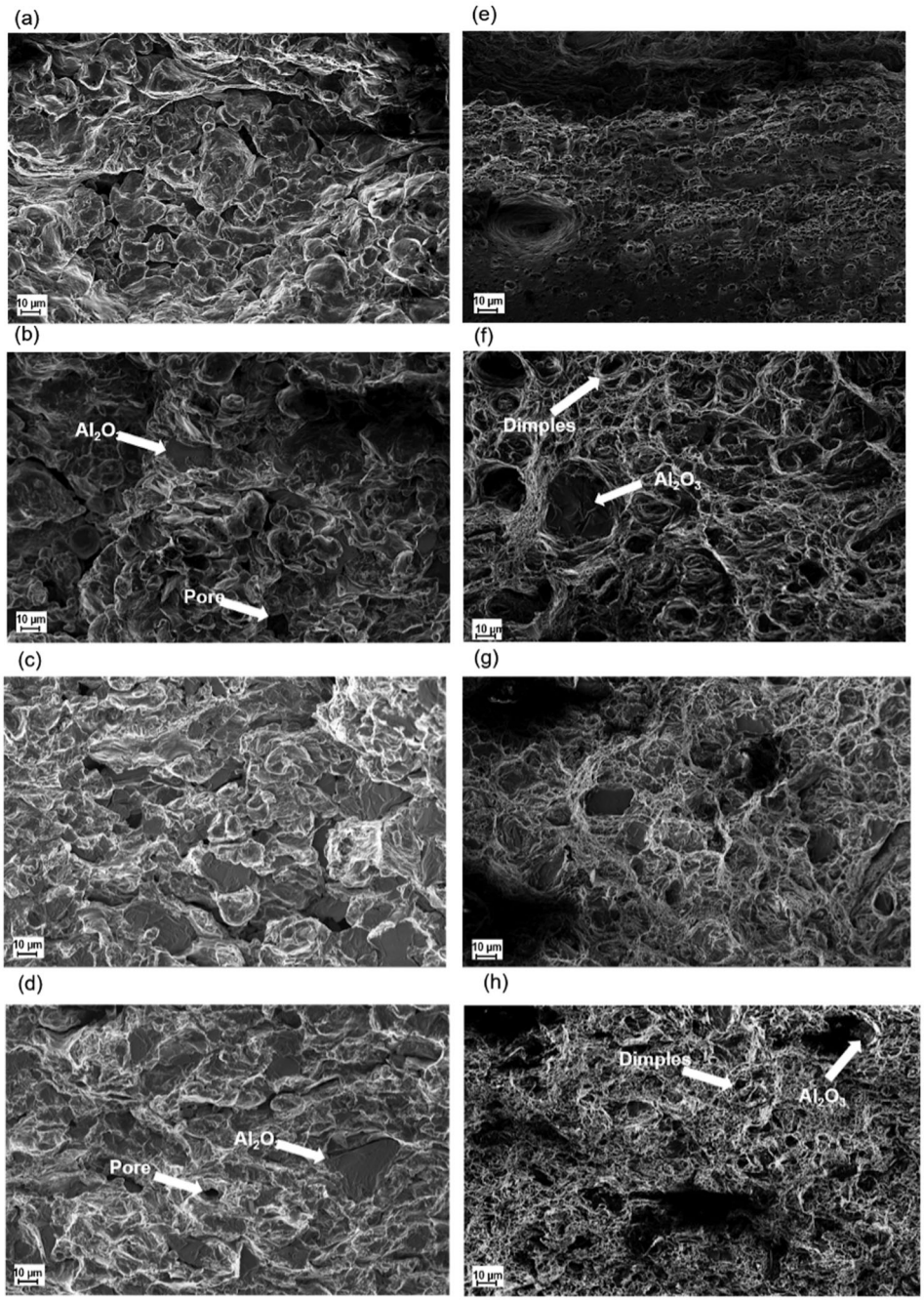

Figure 14. SEM images of the tensile fracture surfaces for as-sprayed coatings with (a) pure Al, (b) 5 wt-% Al_2O_3, (c) 23 wt-% Al_2O_3, (d) 35 wt-% Al_2O_3 and post-FSPed coating with (e) pure Al, (f) 5 wt-% Al_2O_3, (g) 23 wt-% Al_2O_3 and (h) 35 wt-% Al_2O_3.

act as strong nucleation sites for new recrystallised grains that lead to accelerated recrystallisation of Al in the presence of the Al_2O_3 particles. Moreover, the possible disintegration of Al_2O_3 particles and their re-orientation within the metallic matrix post-FSP, resulted in more even distribution of the hard grains in the matrix and higher structural homogeneity that contributed to the improvement of the mechanical properties of the MMC coatings.

Strengthening mechanisms

To better understand the microstructural strengthening mechanisms for cold-sprayed and FSPed MMC coatings, a combined linear law mathematical model was considered. The flow stress for the MMC coatings can be described as follows:

$$\sigma_{FS} = \sigma_{YS} + \sigma_{\rho} + \sigma_{HP} + \sigma_{OR}, \tag{2}$$

where σ_{FS} refers to the flow stress for the MMC coatings. The various contributors to the MMC flow stress include the yield strength contribution from the Al matrix, σ_{YS}, stress contribution due to the dislocation density, σ_{ρ}, the stress contribution due to the matrix grain size according to the Hall-Petch criteria, σ_{HP} and the contribution due to oxide dispersion strengthening or Orowan strengthening, σ_{OR}. The main contribution to the tensile strength of as-sprayed coating is due to Orowan strengthening.

According to the Orowan formula,

$$\sigma_{OR} \propto \frac{\sqrt{v_r}}{\varphi}. \quad (3)$$

The stress contribution from Orowan strengthening is directly proportional to the volume fraction of the Al_2O_3 particles (v_r) and the average size of the Al_2O_3 particles in the coating (φ). Therefore, as the Al_2O_3 content in the coating increases, the tensile strength increases, as more oxide particles create barriers for dislocation movement, thereby resisting plastic deformation. The oxide particles act as dislocation pinning sites, creating additional barriers for dislocation movement, thereby requiring increased force to cause plastic deformation. A similar strengthening phenomenon, synergistic strengthening, was found by Shao et al. [17] who found that increasing ceramic content in an as-sprayed MMC coating improved the yield strength of the coatings due to the improved ceramic content distribution and in-situ strain hardening of the matrix during cold spray deposition. The post-FSPed coatings exhibited increased UTS due to the Al_2O_3 particle sizes being lower than that of as-sprayed coatings with the same Al_2O_3 content. This increases the contribution from Orowan strengthening and produces coatings with higher UTS.

The improved tensile properties of the post-FSPed coatings can also be explained by the additional strengthening effects due to the grain refinement that occurs in the material during FSP. The grain refinement that occurs in the coating matrix decreases the average grain size in the matrix. According to the Hall-Petch criteria,

$$\sigma_{HP} \propto \frac{1}{d}, \quad (4)$$

where d is the distance between adjacent dislocations in the material. As the grain size decreases, due to refinement after FSP, as indicated by the dimpled fracture surfaces, there are more grain boundaries closer together in the matrix, which decreases the value for d thereby increasing the overall strength of the material. Though the contribution from grain refinement is not as large as the contribution from Orowan strengthening, it still contributes to the overall strength of the coatings, yielding higher UTS values for post-FSPed coatings.

The remarkable improvement in the elongation and toughness of the post-FSPed coatings compared to the as-sprayed coatings can be attributed to the strain hardening and recrystallisation of Al that occurs in the material during FSP. To understand the effects of this thermoplastic deformation, a physical constitutive model is considered, which uses the dislocation density, ρ, as an internal variable of the microstructural evolution in the material. According to dislocation density theory [18],

$$\sigma_\rho \propto \sqrt{\rho}. \quad (5)$$

The Kocks and Mecking (K-M) model is used to trace the microstructural evolution in the material. During a thermoplastic deformation process, the microstructural evolution depends on the competition between strain hardening and recrystallisation of the metallic component Al [18]. During strain hardening, materials are strengthened by dislocation multiplication that occurs in the materials, increasing the dislocation density. Increased dislocation density increases resistance to plastic deformation thereby improving the tensile strength of the material. Due to localised elevated temperature and strain rates involved in FSP, the material also undergoes dynamic recovery and recrystallisation [2, 13]. During recrystallisation, the Al in the matrix experiences grain nucleation (refinement) and growth, which leads to dislocation annihilation or reabsorption. This lowers the dislocation density in the material. The K-M model suggests that the dislocation evolution in the material during a thermoplastic deformation process occurs according to the equation:

$$\frac{d\rho}{d\varepsilon} = k_1\sqrt{\rho} - k_2\rho, \quad (6)$$

where k_1 is the strain hardening coefficient and k_2 is the recrystallisation coefficient. The interactive effects of strain hardening and recrystallisation, as experienced in FSP, are responsible for the improved tensile strength and elongation of the post-FSPed coatings. The remarkable enhancement in the elongation of the post-FSPed coatings can be attributed to grain refinement that takes place during recrystallisation. Therefore, during FSP, the impact of Al recrystallisation dominates the effect of strain hardening at high strain rates, since according to the K-M model, the dislocation density decreases in the material, allowing for greater elongation and consequently increased toughness of the coatings.

Abrasive wear behaviour

The wear rate of the as-sprayed and post-FSPed MMC coatings during dry abrasion testing, per ASTM Standard G65 17, is illustrated in Figure 15. Following the inverse trend of the coating hardness, the wear rate decreased with increasing Al_2O_3 content in the coating for both the as-sprayed and post-FSPed conditions. The wear rates were between $85.8 \pm 2.8 \times 10^{-5}$ mm^3/N-m ($n = 3$) and $97.3 \pm 0.9 \times 10^{-5}$ mm^3/N-m ($n = 3$) for the as-sprayed coating samples. Following FSP, the wear rate for the coatings decreased further, yielding the lowest wear rate for the post-FSPed 35 wt-% Al_2O_3 of $81.6 \pm 1.4 \times 10^{-5}$ mm^3/N-m ($n = 3$). Since FSP involves localised elevated temperatures during the process, it can introduce thermal softening into the coating, which can negatively affect the abrasion resistance of the material. However, from the quantitative values of the wear rates for the post-FSPed

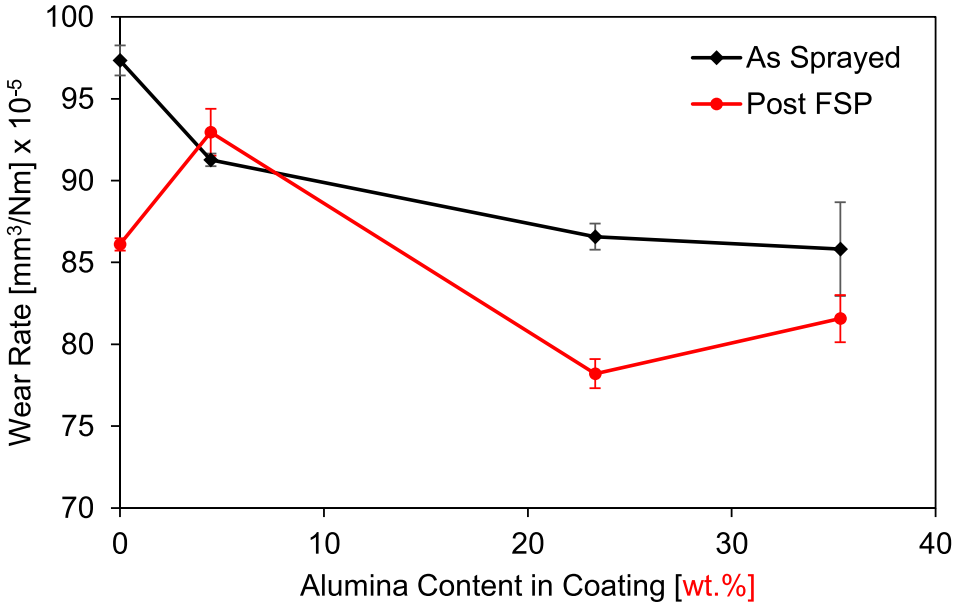

Figure 15. Dry abrasion wear rate versus Al_2O_3 content for as-sprayed and post-FSPed coatings.

coatings, this negative effect of thermal softening was lower than the improvements due to improved consolidation, ceramic particle distribution and interparticle bonding following FSP, which produced a net improvement in wear resistance. The enhanced wear performance of the post-FSPed coatings demonstrates the advantages of FSP for abrasion resistance performance. The reduced mean free path between Al_2O_3 particles after FSP reflects the improved dispersion and refinement of the Al_2O_3 particles in the coating matrix, which increases the hardness of the coating through load sharing. Due to this improved hardness of the coating, the depth of the abrasion is limited, which consequently improves the wear performance of the coating [13]. A similar correlation between hardness and wear performance has been explored for other thermal spray coatings. The pure Al coating experienced a decrease of 13% in the wear rate after FSP. This can be explained by the improved bonding between the Al particles due to the compaction and consolidation effects during FSP. Considering the wear behaviour for the various coatings, it can be suggested that the abrasive particles remove the soft, ductile Al matrix that surrounds the Al_2O_3 particles first. Continued exposure to the abrasive particles causes the hard Al_2O_3 particles to be pulled from the coating surface. This is due to the weak interparticle bonding between the Al and Al_2O_3 particles. Similar wear behaviour was found by Peat et al. [10] with cold-sprayed WC-Co coatings.

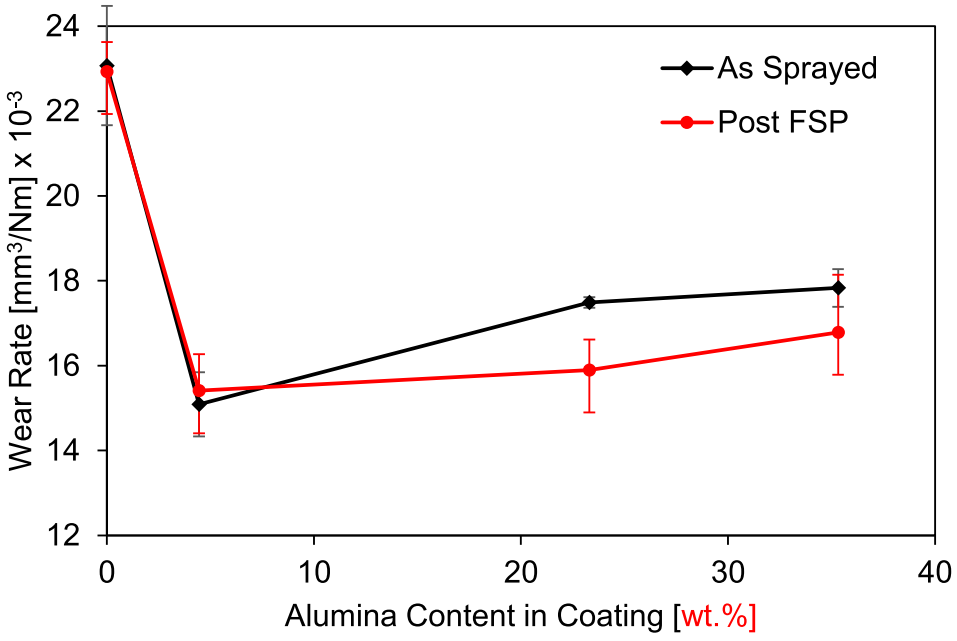

Figure 16. High-stress abrasion wear rate versus Al_2O_3 content for as-sprayed and post-FSPed coatings.

The results from high-stress abrasion testing, as illustrated in Figure 16, indicated that the wear rate for the coatings was three orders of magnitude higher under wet conditions compared to dry. For both as-sprayed and post-FSPed coatings, the wear rate decreased significantly from the pure Al to the 5 wt-% Al_2O_3 coating; however, little variation with increasing Al_2O_3 content was observed afterwards. High-stress abrasion testing involves using a steel wheel and an abrasive slurry which creates stronger embedding of the abrasive particles to the MMC compared to the dry abrasion test assembly resulting in high wear rates.

Conclusions

This study was conducted to propose a novel methodology of repairing high-strength cold-worked aluminium alloys, specifically AA5052-H32, using cold-sprayed Al–Al_2O_3 MMC coating overlays and FSP. The microstructural changes in the overlay after FSP were investigated and the mechanical and wear performance in the as-sprayed state and after FSP were quantified. The strengthening mechanisms for cold-sprayed and FSPed MMC were identified and discussed. The main conclusions from the study are as follows:

(1) FSP enhances the Al_2O_3 particle dispersion in the coating matrix and reduces the porosity compared to as-sprayed coatings due to the stirring and consolidating effects of FSP.
(2) Following FSP, the hardness and ultimate tensile strengths of the coatings were improved due to the enhanced Al_2O_3 particle dispersion and reduced porosity.
(3) FSP leads to remarkable improvement in coating elongation and toughness by reducing physical defects and introducing recrystallisation of Al in the MMC. FSPed coatings experienced ductile failure in comparison to the brittle/premature failure for the as-sprayed coatings.
(4) Cold spray-FSP hybridisation can be considered an effective repair methodology for the currently unrepairable AA5052-H32.

Acknowledgements

The authors would like to thank Mr. Kapil Bhagavathula for hardness testing training and DIC training and Dr. Chenwei Shao for assistance with SEM imaging. The authors extend their gratitude to Mr. David Parlin for assistance with wire EDM, Mr. Mitul Patel for assistance with the tensile testing, and Mr. Maxime Guerin for assistance with the FSP.

Disclosure statement

No potential conflict of interest was reported by the author (s).

Funding

This work was supported by the Natural Sciences and Engineering Research Council of Canada under a Discovery Grant [Number RGPIN-2018-04298].

References

[1] Mishra RS, Ma ZY, Charit I. Friction stir processing: a novel technique for fabrication of surface composite. Mater Sci Eng A. 2003;341(1–2):307–310. doi:10.1016/S0921-5093(02)00199-5.
[2] Yang K, Li W, Niu P, et al. Cold sprayed AA2024/Al_2O_3 metal matrix composites improved by friction stir processing: microstructure characterization, mechanical performance and strengthening mechanisms. J Alloys Compd; 2018(736):115–123.
[3] Nolting AE, Larose S, Cao X, et al. Localized strength restoration of aluminum 5083 with ceramic particles via friction stir processing. Proceedings of the NATO-STO AVT-267 work. future addit. manuf. mil. hardw.; 2018; p. 1–18.
[4] Liu FC, Ma ZY. Achieving exceptionally high superplasticity at high strain rates in a micrograined Al-Mg-Sc alloy produced by friction stir processing. Scr Mater. 2008;59:882–885. doi:10.1016/j.scriptamat.2008.06.035
[5] Champagne V, Helfritch D. Critical assessment 11: structural repairs by cold spray. Mater Sci Technol. 2015;31(6):627–634. doi:10.1179/1743284714Y.0000000723
[6] Sun W, Chu X, Lan H, et al. Current implementation status of cold spray technology: a short review. J Therm Spray Tech. 2022;31(4):848–865. doi:10.1007/s11666-022-01382-4
[7] Lee YTR, Ashrafizadeh H, Fisher G, et al. Effect of type of reinforcing particles on the deposition efficiency and wear resistance of low-pressure cold-sprayed metal matrix composite coatings. Surf Coat Technol. 2017;324:190–200. doi:10.1016/j.surfcoat.2017.05.057
[8] Munday G, Hogan J, McDonald A. On the microstructure-dependency of mechanical properties and failure of low-pressure cold-sprayed tungsten carbide-nickel metal matrix composite coatings. Surf Coat Technol. 2020;396:125947. doi:10.1016/j.surfcoat.2020.125947
[9] Hodder KJ, Izadi H, McDonald AG, et al. Fabrication of aluminum-alumina metal matrix composites via cold gas dynamic spraying at low pressure followed by friction stir processing. Mater Sci Eng A. 2012;556:114–121. doi:10.1016/j.msea.2012.06.066
[10] Peat T, Galloway A, Toumpis A, et al. The erosion performance of cold spray deposited metal matrix composite coatings with subsequent friction stir processing. Appl Surf Sci. 2017;396:1635–1648. doi:10.1016/j.apsusc.2016.10.156
[11] Charit I, Mishra RS. High strain rate superplasticity in a commercial 2024 Al alloy via friction stir processing. Mater Sci Eng A. 2003;359:290–296. doi:10.1016/S0921-5093(03)00367-8
[12] Rao D, Huber K, Heerens J, et al. Asymmetric mechanical properties and tensile behaviour prediction of aluminium alloy 5083 friction stir welding joints. Mater Sci Eng A. 2013;565:44–50. doi:10.1016/j.msea.2012.12.014
[13] Peat T, Galloway A, Toumpis A, et al. Enhanced erosion performance of cold spray co-deposited AISI316 MMCs modified by friction stir processing. Mater Des. 2017;120:22–35. doi:10.1016/j.matdes.2017.01.099

[14] Huang C, Li W, Zhang Z, et al. Modification of a cold sprayed SiCp/Al5056 composite coating by friction stir processing. Surf Coat Technol. 2016;296:69–75. doi:10.1016/j.surfcoat.2016.04.016
[15] Li W, Feng Y, Planche MP, et al. Microstructural evolution and mechanical properties enhancement of a cold-sprayed Cu[sbnd]Zn alloy coating with friction stir processing. Mater Charact. 2017;125:76–82. doi:10.1016/j.matchar.2017.01.027
[16] Travitzky N. Processing of ceramic–metal composites. Adv Appl Ceram. 2012;111(5-6):286–300. doi:10.1179/1743676111Y.0000000073
[17] Shao C, Lo C, Bhagavathula K, et al. High strength particulate aluminum matrix composite design: synergistic strengthening strategy. Compos Commun. 2021;25:100697. doi:10.1016/j.coco.2021.100697
[18] Kocks UF, Mecking H. Physics and phenomenology of strain hardening: the FCC case U.F. Prog Mater Sci. 2002;48:171–273. doi:10.1016/S0079-6425(02)00003-8
[19] ASTM International. G65-16: standard test method for measuring abrasion using the dry sand / rubber wheel. ASTM Stand. 2013;04(Reapproved 2010):1–12. doi:10.1520/G0065-04R10.2
[20] ASTM International. ASTM b611 standard test method for determining the high stress abrasion resistance of hard. ASTM B611. 2017;13(Reapproved 2018):1–6. doi:10.1520/B0611-13.2
[21] ASTM E8. ASTM e8/E8M standard test methods for tension testing of metallic materials 1. Annu B ASTM Stand. 2010;4(C):1–27. doi:10.1520/E0008
[22] Irissou E, Legoux JG, Arsenault B, et al. Investigation of Al-Al 2O 3 cold spray coating formation and properties. J Therm Spray Technol. 2007;16:661–668. doi:10.1007/s11666-007-9086-8
[23] Spencer K, Fabijanic DM, Zhang MX. The use of Al-Al_2O_3 cold spray coatings to improve the surface properties of magnesium alloys. Surf Coat Technol. 2009;204:336–344. doi:10.1016/j.surfcoat.2009.07.032
[24] Xie X, Chen C, Chen Z, et al. Achieving simultaneously improved tensile strength and ductility of a nano-TiB2/AlSi10Mg composite produced by cold spray additive manufacturing. Compos B Eng. 2020;202:108404-1–108404-11. doi:10.1016/j.compositesb.2020.108404.